5328 *Inorg. Chem.* **2010**, *49*, 5328–5334
DOI: 10.1021/ic1004424

Inorganic Chemistry
Article

High-Spin Manganese(II) Complexes of an Amido/Bis(Phosphine) PNP Ligand

Deborha Bacciu,[†] Chun-Hsing Chen,[†] Panida Surawatanawong,[‡] Bruce M. Foxman,[†] and Oleg V. Ozerov*[,†,‡]

[†]*Department of Chemistry, Brandeis University, MS 015, 415 South Street, Waltham, Massachusetts 02454, and* [‡]*Department of Chemistry, Texas A&M University, 3255 TAMU, College Station, Texas 77842.*

Received March 6, 2010

Syntheses of several Mn complexes supported by a monoanionic amido/bis(phosphino) PNP ligand (PNP = [2-P($CHMe_2$)$_2$-4-MeC_6H_3]$_2$N) from anhydrous $MnCl_2$ are reported. Treatment of (PNP)Li (**2**) with $MnCl_2$ in tetrahydrofuran (THF) led to isolation of either (PNP)Mn(μ-Cl)$_2$Li(THF)$_2$ (**5**) or (PNP)MnCl (**6**), depending on the workup. Reaction of **6** with 2 equiv of MeLi resulted in isolation of (PNP)Mn(μ-Me)$_2$Li(THF)$_2$ (**7**) that is structurally similar to **5**. Reduction of **6** in the presence of pyridine produced material analytically consistent with (PNP)Mn(py)$_3$ (**8**), whereas reduction in the presence of 2,2′-bipyridine gave fully characterized (PNP)Mn(bipy) (**9**). Compounds **5** and **7** display magnetic moments indicative of high-spin Mn(II) (S = 5/2). The magnetic moment of **9** (S = 2) was interpreted as an antiferromagnetic combination of a high-spin Mn(II) center and a singly reduced bipyridine ligand. Addition of a single CO ligand to **9** generated diamagnetic, low-spin (PNP)Mn(bipy)(CO) (**10**). Solid-state structures of **5**, **7**, **9**, and **10** were determined by X-ray diffraction methods and used in conjunction with density functional theory studies to analyze the electronic nature of the (PNP)Mn complexes under study.

Introduction

The organometallic chemistry of manganese is dominated by polycarbonyl and cyclopentadienyl complexes on the one hand, and high-spin Mn(II) complexes on the other.[1] In the latter, the metal center interacts with ligands mostly electrostatically and behaves more akin to Zn(II) or Ca(II) complexes than to transition metals.[2] The number of organometallic low-spin Mn complexes that do not bear cyclopentadienyl or multiple carbonyl ligands is small. In general, organometallic Mn complexes in odd oxidation states without cyclopentadienyl or carbonyl ligands are rare as well.[3] Related to these observations is the fact that the most commonly available starting materials for Mn chemistry are $Mn_2(CO)_{10}$ or $(CO)_5MnX$ polycarbonyls or Mn(II) salts. Mn(III) acetylacetonate and acetate (as a hydrate) are also available and have a place in organic synthesis as specialty one-electron oxidants.[4]

Much of the transition metal-based catalysis relies on second- and third-row metals;[5] however, interest in using the more abundant, more economical, and less toxic first-row congeners has been on the rise. Manganese compounds have been successfully used as olefin epoxidation catalysts[6] and organomanganese(II) compounds are an interesting alternative to classical Grignard reagents.[7] However, many typical catalytic organometallic processes (coupling reactions, olefin hydrogenation, cyclization of unsaturates, etc.) depend on oxidative addition/reductive elimination sequences, and manganese has been by and large conspicuously absent from this scene of action.[8]

We recently became interested in the structural, electronic, and reactivity possibilities available to Mn in complexes supported by a diarylamido/bis(phosphino) PNP pincer ligand.[9] We are especially interested in accessing unsaturated Mn complexes with potential for substrate coordination and transformation. In collaboration with the Nocera group, we reported the reactivity of the Mn polycarbonyls supported by the PNP ligand (Scheme 1), with a focus on the ligand-based

*To whom correspondence should be addressed. E-mail: ozerov@chem.tamu.edu.

(1) (a) Sweigart, D. A.; Reingold, J. A.; Son, S. U. In *Comprehensive Organometallic Chemistry III*; Elsevier: Amsterdam, 2007; Vol. *5*, pp 761−813. (b) Sheridan, J. B. In *Comprehensive Organometallic Chemistry III*; Elsevier: Amsterdam, 2007; Vol. *5*, pp 815−831.
(2) Layfield, R. A. *Chem. Soc. Rev.* **2008**, *37*, 1098.
(3) (a) Morris, R. J.; Girolami, G. S. *Organometallics* **1991**, *10*, 792. (b) Morris, R. J.; Girolami, G. S. *Organometallics* **1991**, *10*, 799.
(4) Snider, B. B. *Chem. Rev.* **1996**, *96*, 339.
(5) Van Leeuwen, P. W. N. M. *Homogeneous Catalysis: Understanding the Art*; Kluwer Academic: Dordrecht, The Netherlands, 2004.
(6) McGarrigle, E. M.; Gilheany, D. G. *Chem. Rev.* **2005**, *105*, 1563.
(7) (a) Normant, J.-F.; Cahiez, G. In *Modern Synthetic Methods*; Scheffold, R., Ed.; Otto Salle Verlag GmbH & Co.: Frankfurt am Main, 1983; Vol. *3*, p 173. (b) Cahiez, G.; Mahuteau-Betzer, F. In *Handbook of Functionalized Organometallics: Applications in Synthesis*; Knochel, P., Ed.; Wiley-VCH: Weinheim, Germany, 2005; Vol. *2*, p 541. (c) Oshima, K. *J. Organomet. Chem.* **1999**, *575*, 1.
(8) (a) Teo, Y.-C.; Yong, F.-F.; Poh, C.-Y.; Yan, Y.-K.; Chua, G.-L. *Chem.Commun.* **2009**, *41*, 6258. (b) Tsuji, H.; Yamagata, K.; Fujimoto, T.; Nakamura, E. *J. Am. Chem. Soc.* **2008**, *130*, 7792.
(9) For reviews on the diarylamido-based PNP complexes, see: (a) Liang, L.-C. *Coord. Chem. Rev.* **2006**, *250*, 1152. (b) Ozerov, O. V. In *The Chemistry of Pincer Compounds*; Morales-Morales, D., Jensen, C. M., Eds.; Elsevier: Amsterdam, 2007.

 Published on Web 05/04/2010

Scheme 1

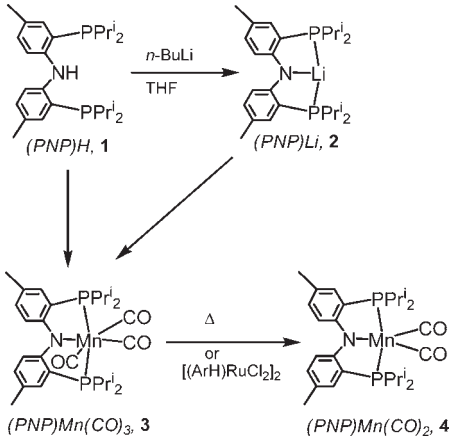

redox chemistry.[10] In that work, we failed to reduce the number of the carbonyls per Mn center past two. Desiring to access carbonyl-free or monocarbonyl Mn complexes, we decided to explore alternative synthetic routes using $MnCl_2$ as the starting material. Here we report the results of our studies that have led us to compounds of non-trivial electronic structure.

Results

Synthesis and Characterization. Deprotonation of (PNP)H (**1**) with ^{n}BuLi in tetrahydrofuran (THF), followed by treatment with $MnCl_2$ resulted in the formation of a yellow solution from which compound **5** was isolated in 91% yield upon workup (Scheme 2). When **5** so obtained was repeatedly recrystallized from THF/pentane mixtures, lithium chloride was eliminated, and a light yellow solid of (PNP)MnCl (**6**) was isolated in analytical purity. Complex **7** was obtained in 31% isolated yield following the treatment of **6** with 2 equiv of MeLi in THF. Compounds **5**−**7** were NMR silent. Ambient temperature Evans method determinations of the solution magnetic moments for **5** (μ_{eff} = 5.8 μ_B) and **7** (μ_{eff} = 5.6 μ_B) were consistent with S = 5/2 states of high spin Mn(II). The ambient temperature magnetic moment determined for **6** (μ_{eff} = 4.9 μ_B) is lower than that expected for Mn(II); it is possible that equilibrium between monomeric and dimeric forms and electronic coupling in the dimer lead to reduced apparent magnetic moment.

Reduction of **6** with NaK in THF in the presence of 3.2 equiv of pyridine led to the isolation of a green paramagnetic solid **8** in 42% yield. Elemental analysis of this solid was consistent with the empirical formula for (PNP)-Mn(py)$_3$. Treatment of bipyridine with 1 equiv of Li metal in THF, followed by addition of **6**, resulted in the formation of brown **9**, which was isolated in analytical purity in 80% yield. Both **8** and **9** were NMR silent. The magnetic moment for **9** determined by the Evans method in solution (μ_{eff} = 4.5 μ_B, ambient temperature) pointed to an S = 2 state. We also determined the magnetic moment for **8** (μ_{eff} = 5.2 μ_B, ambient temperature); however, its interpretation is hampered by the lack of firm structural information on this compound.

(10) Radosevich, A. T.; Melnick, J. G.; Stoian, S. A.; Bacciu, P. D.; Chen, C.-H.; Foxman, B. M.; Ozerov, O. V.; Nocera, D. G. *Inorg. Chem.* **2009**, *48*, 9214.

Scheme 2

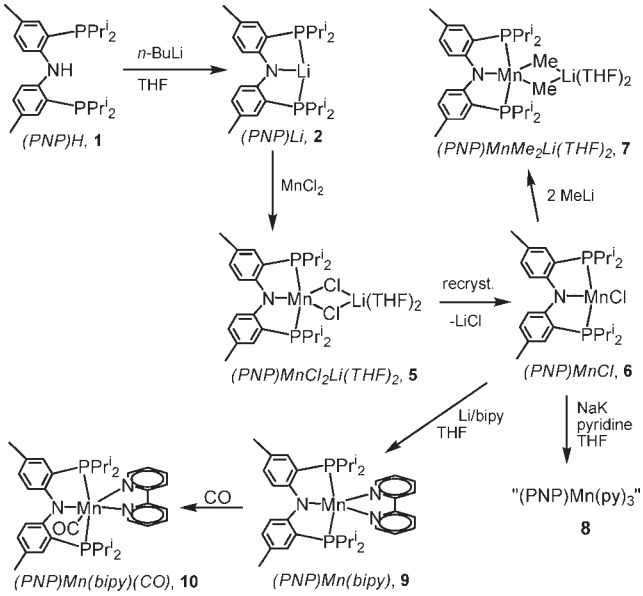

Exposure of the THF solution of **9** to CO atmosphere led to a change of the color of the solution to purple. The purple solid **10** was isolated in 92% yield upon workup. **10** is diamagnetic and displays rather complicated ^{1}H and ^{13}C NMR spectra with a number of overlapping signals. It is likely that the bipyridine "wedge" slows down the conformational movements that would in a fast regime result in an apparent C_s symmetry for **10**. The observed number of signals is greater than that expected for C_s, indicative of C_1 symmetry, with multiple overlaps. **10** displays a single resonance in the ^{31}P NMR spectrum at δ 68.0 ppm, presumably an accidental overlap of two inequivalent signals. The IR band corresponding to the CO stretching vibration appears at a low frequency (ν_{CO} = 1815 cm^{-1}).

Structures. The structures of compounds **5**, **7**, **9**, and **10** were determined by single crystal X-ray diffraction methods (Figures 1−4). In the structures of **5** (Figure 1) and **7** (Figure 2), the coordination environment about Mn is irregular five-coordinate and cannot be assigned either a trigonal bypyramidal (TBP) or a square pyramidal formalism. The angles about the Mn centers in these two compounds vary in the 95−150° range. In **9** (Figure 3), the coordination environment about Mn is recognizably TBP with the amido nitrogen and one of the bipyridine nitrogens occupying the axial positions, and the deviations from idealized TBP angles likely owing to the constraints of the chelating ligands. In the structure of **10** (Figure 4), the donor atoms form an approximate octahedron about Mn, with deviations, again, ostensibly arising from chelate constraints.

The most striking contrast among the metrics of these four different structures is evident in the Mn−P bond lengths in compound **10** versus those in compounds **5**, **7**, and **9**. In **10**, the Mn−P distances are about 2.30 Å, whereas the Mn−P distances are in the range of 2.57−2.64 Å in **5** and **9**, and even longer (2.73−2.74 Å) in **7**. The Mn−N$_{amido}$ bond distances are also shortest in compound **10**, but the difference with **5**, **7**, and **9** is less dramatic (ca. 2.09 Å for **10** and ca. 2.12−2.17 Å for **5**, **7**,

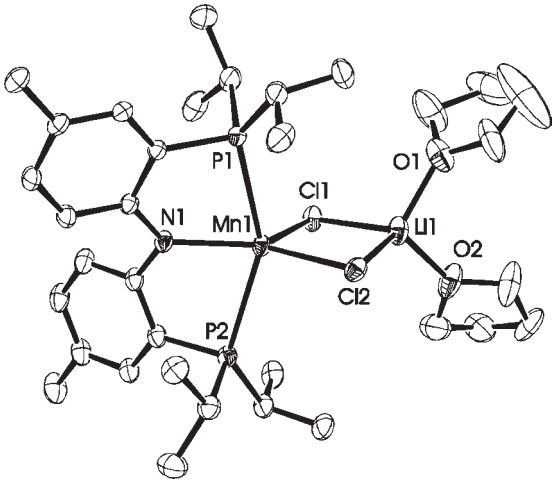

Figure 1. ORTEP drawing[11] (30% probability ellipsoids) of (PNP)$MnCl_2$-$Li(THF)_2$ (**5**) showing selected atom labeling. Hydrogen atoms, the disorder of one of the THF units, and the pentane solvent molecule are omitted for clarity. Selected bond distances (Å) and angles (deg) follow: Mn1−Cl1, 2.4115(6); Mn1−Cl2, 2.4576(6); Mn1−P1, 2.6047(6); Mn1−P2, 2.6049(6); Mn1−N1, 2.154(2), Cl1−Mn1−Cl2, 95.69(2); Cl1−Mn1−P1, 100.37(2); Cl2−Mn1−P1, 98.87(2); Cl1−Mn1−P2, 104.97(2); Cl2−Mn1−P2, 97.00(2); P1−Mn1−P2, 148.46(2); Cl1−Mn1−N1, 119.55(5); Cl2−Mn1−N1, 144.77(5); P1−Mn1−N1, 75.78(5); P2−Mn1−N1, 75.53(5).

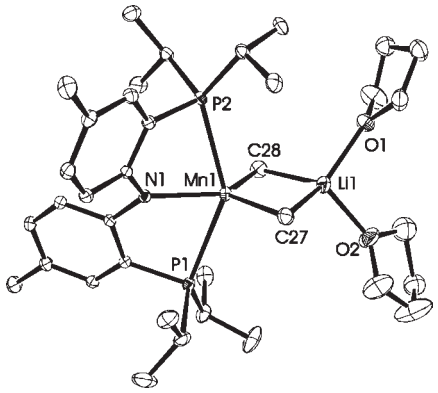

Figure 2. ORTEP drawing[11] (30% probability ellipsoids) of one of the two independent molecules of (PNP)$MnMe_2Li(THF)_2$ (**7**) showing selected atom labeling. Hydrogen atoms, free THF solvent molecules, and the disorder of free and bound THF molecules are omitted for clarity. Selected bond distances (Å) and angles (deg) follow: Mn1−P1, 2.7250(7); Mn1−P2, 2.7379(7); Mn1−N1, 2.164(2); Mn1−C27, 2.203(3); Mn1−C28, 2.201(3); Mn1···Li1, 2.633(5); P1−Mn1−P2, 145.17(2); P1−Mn1−C27, 102.08(8); P2−Mn1−C27, 97.61(10), N1−Mn1−C27, 118.21(10); P1−Mn1−C28, 100.00(8); P2−Mn1−C28, 98.88(8); N1−Mn1−C28, 129.81(10); C27−Mn1−C28, 111.90(12).

and **9**). The two $Mn-N_{bipy}$ distances in **10** differ by about 0.1 Å; this disparity likely occurs because the two bipyridine N donors are disposed *trans* to ligands of different *trans* influence: CO and N_{amido}. CO is a stronger *trans* influence ligand and corresponds to longer $Mn-N_{bipy}$ distance *trans* to it. Yet, even this longer $Mn-N_{bipy}$ distance in **10** (2.0660(15) Å) is shorter than either $Mn-N_{bipy}$ distance in **9** (2.1267(12) and 2.1079(12) Å), although the difference is again not as dramatic as with the Mn−P bond distances.

Discussion

Electronic Structure of Mn Compounds. Complexes **5** and **7** can be unambiguously described as high-spin Mn(II)

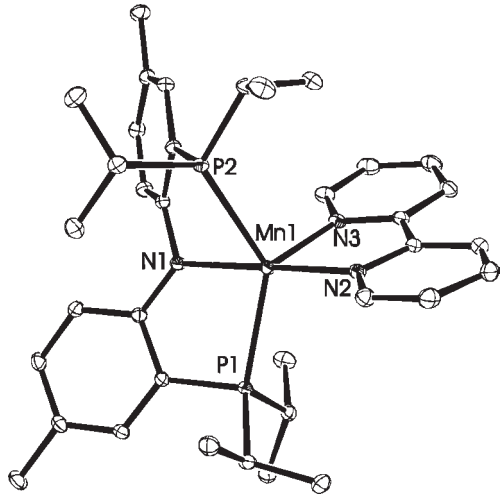

Figure 3. ORTEP drawing[11] (30% probability ellipsoids) of (PNP)Mn-(bipy) (**9**) showing selected atom labeling. Hydrogen atoms and the free THF solvent molecule are omitted for clarity. Selected bond distances (Å) and angles (deg) follow: Mn1−P1, 2.5734(4); Mn1−P2, 2.6341(4); Mn1−N1, 2.1229(12); Mn1−N2, 2.1267(12); Mn1−N3, 2.1079(12); P1−Mn1−P2, 137.311(14); P1−Mn1−N1, 77.00(3); P2−Mn1−N1, 74.79(3); P1−Mn1−N2, 103.63(3); P2−Mn1−N2, 102.02(3); N1−Mn1−N2, 175.11(5); P1−Mn1−N3, 115.41(4); P2−Mn1−N3, 103.29(4); N1−Mn1−N3, 107.39(5); N2−Mn1−N3, 76.82(5).

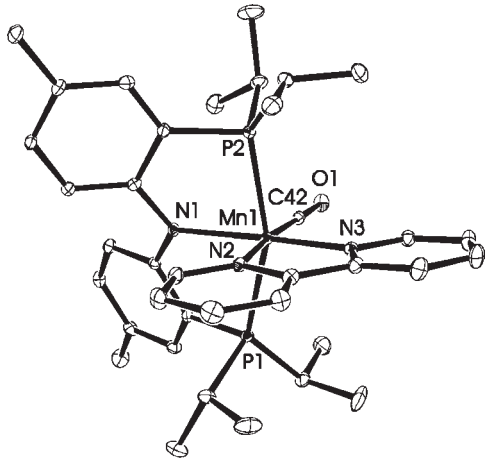

Figure 4. ORTEP drawing[11] (30% probability ellipsoids) of (PNP)Mn(bipy)(CO) (**10**) showing selected atom labeling. Hydrogen atoms and the pentane solvent molecule are omitted for clarity. Selected bond distances (Å) and angles (deg) follow: Mn1−P1, 2.2987(5); Mn1−P2, 2.2912(5); Mn1−N1, 2.0907(15); Mn1−N2, 2.0660(15); Mn1−N3, 1.9623(16); Mn1−C42, 1.7508(18); P1−Mn1−P2, 156.71(2); N1−Mn1−N3, 168.76(6); N2−Mn1−C42, 171.89(8).

compounds. The composition and connectivity of these complexes, together with solution magnetic moment determinations, provide sufficient support for such assignment. On the other hand, for complex **10**, the "diamagnetic" NMR spectra alone strongly suggest a closed shell, low-spin Mn(I) nature. The electronic structure of **9** is less easily pinned down. Its formulation as (PNP)Mn(bipy) at first glance suggests a Mn(I) center with an anionic PNP ligand and a neutral bipyridine ligand. The solution magnetic moment indicates an $S = 2$ state. If based on the unpaired electrons from the metal alone, it would necessitate an exotic high-spin Mn(I) configuration. A Mn(I) center without any significant π-acid ligands would be powerfully reducing. Both PNP and bipy are redox-non-innocent

ligands, but PNP is rather susceptible to *oxidation*,[10,12] not reduction. Bipyridine, on the other hand, can accept an electron from strongly reducing agents: it is easily reduced by alkali metals[13] and compounds such as Herzog's $Ti(bipy)_3$ and Roesky's $[Al(bipy)_2]^-$ contain multiple reduced bipyridines about a metal center.[14,15] Thus, an alternative formulation that emerges for **9** is one with a high-spin Mn(II) center antiferromagnetically coupled to the unpaired electron in a singly reduced bipyridine. Analogous intramolecular reduction of bipyridine by a low-valent metal center has been closely scrutinized in the chemistry of lanthanides. For example, complexes $Cp^*_2Yb(bipy)$ containing a reduced bipyridine ligand and $[Cp^*_2Yb(bipy)]^+$ with a "normal" bipyridine ligand (and their close substitutional relatives) have been structurally characterized and studied computationally.[16] The intrabipy distances in the reduced bipyridine in $Cp^*_2Yb(bipy)$ differ meaningfully from those in the ostensibly unperturbed bipyridine in $[Cp^*_2Yb(bipy)]^+$. These variations can be rationalized by considering the effect of populating the π^* orbital in bipyridine. Such analysis has also been used for identification of reduced bipyridine ligands in related Sm, La, and U complexes;[17] however, it does not appear to be applicable when considering the bipyridine fragment in **9** versus **10**. The differences in the intrabipy distances are less pronounced than in the Yb complexes, and do not clearly follow the same trend. This is likely because the bipyridine ligand in $[Cp^*_2Yb(bipy)]^+$ is attached to a purely Lewis acidic metal, while in **10** the bipyridine ligand is attached to a very electron-rich Mn(I) center. The intrabipy metrics in $[Cp^*_2Yb(bipy)]^+$ resemble those of free bipyridine closely;[13] the intrabipy metrics in **10** do not. The likely mixing between π^* orbitals of bipyridine and d_π orbitals of Mn(I) probably distorts the intrabipy distances enough from the "unperturbed" distances that it renders the comparative analysis of the reduced bipyridine in **9** and the π-acceptor bipyridine in **10** uninformative.

The rather extreme degree of electron-richness of the Mn center in **10** is illustrated by the very low stretching frequency observed for the CO ligand ($\nu_{CO} = 1815\,cm^{-1}$). The low value can be understood as a consequence of the low oxidation state of a midperiodic transition metal in a complex where CO is the only strong π-acceptor. In an electronically similar situation but with a 5d metal, Harman et al. reported a series of TpRe(L)(L′)(CO) (Tp = hydridotris(pyrazolyl)borate) where the L and L′ ligands were either weak π-acceptors or pure σ-donors (trilakylphosphines, N-donors, olefins, etc.) in which ν_{CO} values were found to be in the range of $1775-1825\,cm^{-1}$.[18]

Table 1. B3LYP Relative Enthalpies and Free Energies (kcal/mol) and Selected Geometry Parameters of (PNP)Mn(bipy) (**9**) in Singlet, Triplet, and Quintet Spin States

	exp	B3LYP		
	$S = 2$	$S = 0$	$S = 1$	$S = 2$
Relative Energy (kcal/mol)				
ΔH		45.31	20.64	0.00
ΔG		49.69	23.69	0.00
Geometry Parameters (Å, degree)				
Mn1−N1	2.1229(12)	2.138	2.029	2.156
Mn1−P1	2.5734(4)	2.392	2.419	2.650
Mn1−P2	2.6341(4)	2.355	2.497	2.701
Mn1−N2	2.12767(12)	1.951	2.037	2.169
Mn1−N3	2.1079(12)	1.956	2.101	2.131
N3−Mn1−P2	103.29(4)	98.9	103.8	106.6

The structural data are generally in support of **9** having a high-spin Mn center. The low-spin **10** displays the shortest distances to the donor atoms of the PNP ligand among the structurally characterized **5**, **7**, **9**, and **10**. The difference is profound (0.3−0.4 Å) for Mn−P distances and cannot be rationalized on the basis of steric effects, different coordination numbers, or trans influence arguments alone; in fact, **10** has both the highest coordination number and the most congested environment about Mn. **10** is a low-spin Mn(I) compound in which the d_σ orbitals are empty and fully available for making bonds to the two-electron donor ligands. The Mn−P distances in **10** are similar to those observed in $(PNP)Mn(CO)_3$ (**3**) (ca. 2.28 Å), also a low-spin Mn(I) complex. In a high-spin Mn(I) or Mn(II) case, all d orbitals are at least half-occupied and thus the bonds to ligands are inevitably weaker and longer. Wilkinson and Hursthouse reported a series of Mn(II) alkyl complexes with phosphines.[19] In the tetrahedral, high-spin Mn(II) complex $(Me_3P)_2Mn(CH_2CMe_2Ph)_2$, the Mn−P distances were about 2.63 Å, while in the octahedral, low-spin Mn(II) complex $(dmpe)_2Mn(o\text{-}(CH_2)_2C_6H_4)$, the Mn−P distances were in the 2.23−2.30 Å range. The same groups also reported high-spin Mn(II) complexes $Cp_2Mn(PR_3)$ and $Cp_2Mn(dmpe)$, in which the Mn−P distances were in the range of 2.57−2.67 Å.[20] On the other hand, the Mn−P distance in the low-spin Mn(I) complex $CpMn(CO)_2(PPh_3)$ was determined by Ricard and co-workers to be about 2.23 Å.[21] Thus, the Mn−PNP ligand distances place **9** squarely with the high-spin complexes **5** and **7**.

Computational Analysis. To assess our conclusions regarding the electronic structure of **9** and **10**, we undertook a density functional theory (DFT) study. To begin, we optimized the geometries for $S = 0$, $S = 1$, and $S = 2$ states for **9** and **10**. The resultant key metrics and the

(11) ORTEP plots were created using Ortep-3 for Windows. Farugia, L. *J. Appl. Crystallogr.* **1997**, *30*, 565.
(12) Adhikari, D.; Mossin, S.; Basuli, F.; Huffman, J. C.; Szilagyi, R. K.; Meyer, K.; Mindiola, D. J. *Inorg. Chem.* **2008**, *130*, 3676.
(13) For reduction of bipyridine with Li, see: Herzog, S.; Grimm, U. *Z. Chem.* **1968**, *8*, 186.
(14) (a) Herzog, S.; Taube, R. *Z. Anorg. Allg. Chem.* **1960**, *306*, 159. (b) Flamini, A.; Giuliani, A. M. *Inorg. Chim. Acta* **1986**, *112*, L7.
(15) Nikiforov, G. B.; Roesky, H. W.; Noltemeyer, M.; Schmidt, H.-G. *Polyhedron* **2004**, *23*, 561.
(16) (a) Schultz, M.; Boncella, J. M.; Berg, D. J.; Tilley, T. D.; Andersen, R. A. *Organometallics* **2002**, *21*, 460. (b) Booth, C. H.; Walter, M. D.; Kazhdan, D.; Hu, Y.-J.; Lukens, W. W.; Bauer, E. D.; Maron, L.; Eisenstein, O.; Andersen, R. A. *J. Am. Chem. Soc.* **2009**, *131*, 6480.
(17) (a) Evans, W. J.; Drummond, D. K. *J. Am. Chem. Soc.* **1989**, *111*, 3329. (b) Roitershtein, D.; Domingos, Â.; Pereira, L. C. J.; Ascenso, J. R.; Marques, N. *Inorg. Chem.* **2003**, *42*, 7666. (c) Kraft, S. J.; Fanwick, P. E.; Bart, S. C. *Inorg. Chem.* **2010**, *49*, 1103.
(18) Meiere, S. H.; Brooks, B. C.; Gunnoe, T. B.; Carrig, E. H.; Sabat, M.; Harman, W. D. *Organometallics* **2001**, *20*, 3661.
(19) Howard, C. G.; Girolami, G. S.; Wilkinson, G.; Thornton-Pett, M.; Hursthouse, M. B. *J. Am. Chem. Soc.* **1983**, *12*, 2631.
(20) Howard, C. G.; Girolami, G. S.; Wilkinson, G.; Thornton-Pett, M.; Hursthouse, M. B. *J. Am. Chem. Soc.* **1984**, *106*, 2033.
(21) Barbeau, C.; Dichmann, K. S.; Richard, L. *Can. J. Chem.* **1973**, *51*, 3027.

Table 2. B3LYP Relative Enthalpies and Free Energies (kcal/mol), Selected Geometry Parameters, and CO Vibrational Frequency of (PNP)Mn(bipy)(CO) (**10**) in Singlet, Triplet, and Quintet Spin States

	exp	B3LYP		
	$S = 0$	$S = 0$	$S = 1$	$S = 2$
Relative Energy (kcal/mol)				
ΔH		0.00	6.65	13.92
ΔG		0.00	4.05	8.61
Geometry Parameters (Å)				
Mn−N1	2.0907(15)	2.134	2.050	2.006
Mn−P1	2.2987(5)	2.377	2.428	2.801
Mn−P2	2.2912(5)	2.391	2.437	2.824
Mn−N2	2.0660(15)	2.101	2.100	2.048
Mn−N3	1.9623(16)	2.020	2.047	2.054
Mn−C	1.7508(18)	1.763	1.792	1.906
C−O	1.173(2)	1.177	1.166	1.157
CO Vibrational Frequency (cm^{-1})[a]				
ν C1−O1	1815	1838.9	1904.4	1945.6

[a] Scaling factor = 0.9648 is applied to the calculated CO frequency according to Merrick et al.[22]

relative enthalpies and free energies from B3LYP are presented in Tables 1 and 2. The calculated geometries of the ground spin state are shown in Supporting Information, Figure S1. B3LYP calculations confirm our conclusions based on the experimental data of the $S = 2$ state for **9** and $S = 0$ state for **10**. The same conclusions were also reached when using TPSS, a nonhybrid functional (see Supporting Information).

The calculated energy preference for the $S = 2$ state for **9** is quite definitive. In addition, the calculated bond distances for $S = 2$ most closely reproduce the experimental data. Given that B3LYP typically overestimates bond distances by a few hundredths of an angstrom, the calculated distances for $S = 1$ and $S = 0$ states are in irreconcilable disagreement with the experimentally determined ones. This is especially apparent for the Mn−P distances which are fully 0.2−0.3 Å off in the calculated $S = 1$ and $S = 0$ geometries, and to a lesser, but still significant, extent for the $Mn-N_{bipy}$ distances.

The calculated energies for the three spin states of **10** are closer than those for **9**; however, the $S = 0$ state is nonetheless of the lowest energy. The analysis of the metrics, on the other hand, is no less convincing than in the case of **9**. Again, the Mn−P distances are most diagnostic, with the $S = 0$ calculation unequivocally providing the best match for the experimental data. Another parameter that is best reproduced for $S = 0$ is the 0.1 Å difference between the two $Mn-N_{bipy}$ bond distances; this difference is halved in the $S = 1$ calculation and disappears altogether in the $S = 2$ calculation. We have also calculated the frequency of the stretching vibration of the coordinated CO, applying a scaling factor for B3LYP as suggested by Merrick et al.[22] The $S = 0$ calculation gives the best agreement ($\nu_{CO} = 1839\ cm^{-1}$) with the experimentally observed $\nu_{CO} = 1815\ cm^{-1}$. The calculated C−O bond distance for $S = 0$ state is also in the best agreement with the experimentally determined C−O bond distance in **10**; the C−O distances calculated for the $S = 1$ and $S = 2$ states are too short.

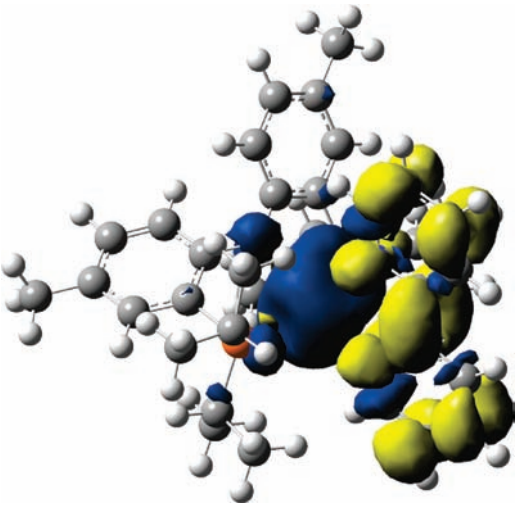

Figure 5. Spin density contour plot for **9** ($S = 2$). The isodensity value is 0.001 (blue for spin up and yellow for spin down). Group spin populations on Mn = 4.818, bipy = −0.906, *N*-diaryl = 0.024, and $2P^iPr_2$ = 0.064.

We also used DFT methods to address the nature of the $S = 2$ state of **9**. Figure 5 shows a plot of the calculated Mulliken spin density in **9**. Calculations show that the spin density is primarily located on the Mn atom and on the bipyridine ligand. The orientation of the spin of the unpaired electron on bipyridine is opposite to those localized on Mn. The spin population analysis suggests five unpaired electrons on Mn (+4.818) and one unpaired electron on bipyridine (−0.906).

Because of the spin polarization effect, spin-coupled orbitals can be difficult to identify from the spin-unrestricted calculation. For a better display, the corresponding orbital transformation[23] as implemented in the ORCA program package[24] is applied to the $S = 2$ state of **9** to arrange each spin-up orbital to overlap the most with each spin-down orbital. The molecular orbitals are ordered into pairs of maximum similarity between spin-up and spin-down orbitals and can be separated into (1) doubly occupied orbitals with spatial overlap close to unity, (2) spin-coupled pairs with spatial overlap significantly smaller than unity, and (3) singly occupied orbitals, which are unmatched orbitals.[20,25] As shown in Figure 6, all four singly occupied orbitals in **9** are of Mn d-orbital characters whereas a spin-coupled pair is a Mn d_π-orbital and a bipyridine orbital with a spatial overlap of 0.51. Thus, calculations support the description of **9** as a complex with a high-spin Mn(II) center with a singly reduced bipyridine ligand and antiferromagnetic coupling between the Mn(II) unpaired electrons and the bipyridine one.

Given our findings concerning the electronic structure of **9**, it seems prudent to expect that complex **8** does not simply contain a Mn^I with three unperturbed pyridine

(22) Merrick, J. P.; Moran, D.; Radom, L. *J. Phys. Chem. A* **2007**, *111*, 11683.
(23) Neese, F. *J. Phys. Chem. Solids* **2004**, *65*, 781.
(24) Neese, F.; Becker, U.; Ganyushin, D.; Hansen, A.; Liakos, D.; Kollmar, C.; Kossmann, S.; Petrenko, T.; Reimann, C.; Riplinger, C.; Sivalingam, K.; Wezisla, B.; Wennmohs, F. *ORCA - an ab initio, DFT and semiempirical electronic structure package*, 2.7; Universität Bonn: Bonn, Germany, 2009.
(25) Kirchner, B.; Wennmohs, F.; Ye, S.; Neese, F. *Curr. Opin. Chem. Biol.* **2007**, *11*, 134.

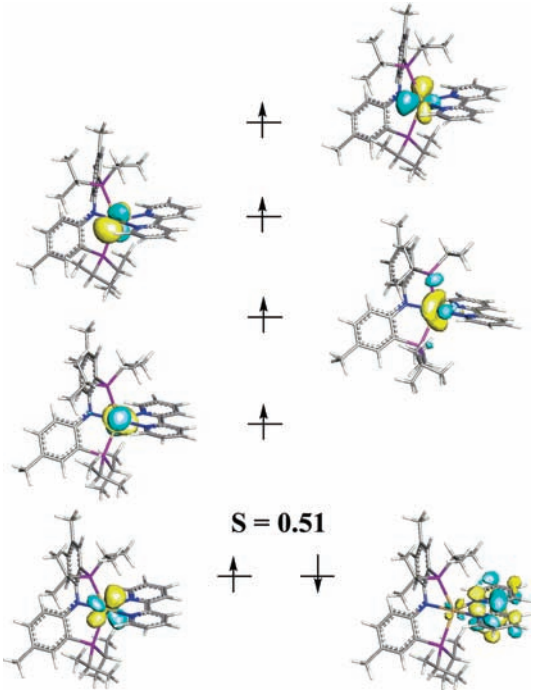

Figure 6. MO scheme for $S = 2$ state of **9**, showing a high spin Mn(II) and a bipyridine anion radical.

donors bound to it. Intramolecular reduction of the pyridine ligands is likely; however, unlike bipyridine, a single pyridine ring is not suited to accept an electron without further rearrangement. For example, Rothwell and co-workers described adducts of low-valent Ti adducts with both bipyridine and pyridine.[26] Whereas bipyridine maintained its integrity, reduction of pyridine ligands led to C−C coupling in the para position. It is possible that related coupling takes place in **8**, but at present this remains a conjecture.

Conclusion

In summary, we have utilized $MnCl_2$ to prepare both high- and low-spin Mn complexes supported by the diarylamido-based PNP pincer ligand. The PNP ligand itself does not enforce the low-spin configuration for Mn(II). The high-spin Mn(II) nature of the metal center in a PNP complex is retained even upon reduction, at the expense of reducing the bipyridine ligand in (PNP)Mn(bipy) (**9**). On the other hand, addition of a single CO ligand profoundly alters the spin-state preference of the metal complex. While **9** prefers a quintet $S = 2$ state (and quite emphatically so, according to our calculations), its CO adduct **10** instead prefers a singlet $S = 0$ state. The change is even more remarkable as not only is the spin state altered, but the formal reduction of Mn(II) by the bipyridine anion takes place. This is a stark manifestation of the textbook declarations of CO being a strong field ligand and a strong π-acid: CO enforces a low-spin configuration and "draws" an extra electron from a ligand to the metal. From another perspective, in the reaction with CO, **9** behaves as a latent source or a synthetic equivalent of the unstable low-spin (PNP)Mn^{I}(bipy). It is possible that it can display this behavior in other reactions as well. Given the strongly reducing nature of this Mn fragment, its reactions with other small molecules may give rise to unusual results.

Experimental Section

General Considerations. Unless specified otherwise, all manipulations were performed under an argon atmosphere using standard Schlenk line or glovebox techniques. Toluene and pentane were dried and deoxygenated (by purging) using a solvent purification system by MBraun and stored over molecular sieves in an Ar-filled glovebox. C_6D_6, toluene-d_8, diethyl ether, and THF were dried over and distilled from NaK/Ph_2CO/18-crown-6 and stored over molecular sieves in an Ar-filled glovebox. Hexamethyldisiloxane was dried over and distilled from Na/K and stored over molecular sieves in an Ar-filled glovebox. $MnCl_2$ was dried with $SOCl_2$ and then under vacuum for 10 h at 200 °C. (PNP)H was synthesized as previously described.[27] All other chemicals were used as received from vendors. NMR spectra were recorded on a Varian iNova 400 (^{1}H NMR, 399.755 MHz; ^{13}C NMR, 100.518 MHz; ^{31}P NMR, 161.822 MHz; ^{19}F NMR, 376.104 MHz) spectrometer. Chemical shifts are reported in δ ppm. For ^{1}H and ^{13}C NMR spectra, the residual solvent peak was used as an internal reference. ^{31}P NMR spectra were referenced externally using 85% H_3PO_4 at 0 ppm. ^{19}F NMR spectra were referenced externally using 80% freon in $CDCl_3$ at −2.3 ppm. Elemental analyses were performed by CALI, Inc. (Parsippany, NJ). All Evans method measurements were performed at ambient temperature.

Computational Details. All geometry optimization and frequency calculations were performed with the Gaussian03 program.[28] B3LYP[29−31] density functional was used for the calculations of **9** and **10** with Stuttgart relativistic small core (RSC) 1997 ECP basis set[32] is used for Mn; LANL2DZdp[33] with effective core potential (ECP) is used for P; 6-31++G(d,p)[34−36] is used for N, O, and C (in CO); and 6-31G(d)[34−36] is used for other C and H. TPSS functional with the same set of basis functions was also performed for a comparison, in which the geometric and energetic results are presented in the Supporting Information. All structures were fully optimized with default convergence criteria, and frequencies were calculated to ensure that there is no imaginary frequency for minima. Zero point energies and thermodynamic

(26) Durfee, L. D.; Fanwick, P. E.; Rothwell, I. P.; Folting, K.; Huffman, J. C. *J. Am. Chem. Soc.* **1987**, *109*, 4720.

(27) Fan, L.; Foxman, B. M.; Ozerov, O. V. *Organometallics* **2004**, *23*, 326.

(28) Frisch, M. J.; Trucks, G. W.; Schlegel, H. B.; Scuseria, G. E.; Robb, M. A.; Cheeseman, J. R.; Montgomery, J. A., Jr.; Vreven, T.; Kudin, K. N.; Burant, J. C.; Millam, J. M.; Iyengar, S. S.; Tomasi, J.; Barone, V.; Mennucci, B.; Cossi, M.; Scalmani, G.; Rega, N.; Petersson, G. A.; Nakatsuji, H.; Hada, M.; Ehara, M.; Toyota, K.; Fukuda, R.; Hasegawa, J.; Ishida, M.; Nakajima, T.; Honda, Y.; Kitao, O.; Nakai, H.; Klene, M.; Li, X.; Knox, J. E.; Hratchian, H. P.; Cross, J. B.; Adamo, C.; Jaramillo, J.; Gomperts, R.; Stratmann, R. E.; Yazyev, O.; Austin, A. J.; Cammi, R.; Pomelli, C.; Ochterski, J. W.; Ayala, P. Y.; Morokuma, K.; Voth, G. A.; Salvador, P.; Dannenberg, J. J.; Zakrzewski, V. G.; Dapprich, S.; Daniels, A. D.; Strain, M. C.; Farkas, O.; Malick, D. K.; Rabuck, A. D.; Raghavachari, K.; Foresman, J. B.; Ortiz, J. V.; Cui, Q.; Baboul, A. G.; Clifford, S.; Cioslowski, J.; Stefanov, B. B.; Liu, G.; Liashenko, A.; Piskorz, P.; Komaromi, I.; Martin, R. L.; Fox, D. J.; Keith, T.; Al-Laham, M. A.; Peng, C. Y.; Nanayakkara, A.; Challacombe, M.; Gill, P. M. W.; Johnson, B.; Chen, W.; Wong, M. W.; Gonzalez, C.; Pople, J. A. *Gaussian 03*, Revision B.4, B.5, and C.1; Gaussian, Inc.: Pittsburgh, PA, 2003.

(29) Becke, A. D. *J. Chem. Phys.* **1993**, *98*, 5648.

(30) Lee, C.; Yang, W.; Parr, R. G. *Phys. Rev. B* **1988**, *37*, 785.

(31) Stephens, P. J.; Devlin, F. J.; Chabalowski, C. F.; Frisch, M. J. *J. Phys. Chem.* **1994**, *98*, 11623.

(32) Bergner, A.; Dolg, M.; Kuumlchle, W.; Stoll, H.; Preuszlig, H. *Mol. Phys.* **1993**, *80*, 1431.

(33) Wadt, W. R.; Hay, P. J. *J. Chem. Phys.* **1985**, *82*, 284.

(34) Hariharan, P. C.; Pople, J. A. *Theor. Chim. Acta* **1973**, *28*, 213.

(35) Petersson, G. A.; Al-Laham, M. A. *J. Chem. Phys.* **1991**, *94*, 6081.

(36) Petersson, G. A.; Bennett, A.; Tensfeldt, T. G.; Al-Laham, M. A.; Shirley, W. A.; Mantzaris, J. *J. Chem. Phys.* **1988**, *89*, 2193.

functions were calculated at 298.15 K and 1 atm. Note that the optimized geometry for the $S = 2$ state of **9** was taken for a single point energy calculation by B3LYP with def2-TZVP(-f)[37,38] basis set on Mn, P, and N, and def2-SVP[39,16] basis set on C and H in the ORCA program package[21] to obtain the corresponding orbitals displayed in Figure 6.

X-ray Diffraction Studies. All operations were performed on a Bruker-Nonius Kappa Apex2 diffractometer, using graphite-monochromated MoKα radiation. All diffractometer manipulations, including data collection, integration, scaling, and absorption corrections were carried out using the Bruker Apex2 software.[40] The structures were solved using SIR-92,[41] and refined (full-matrix-least-squares) using the Oxford University *Crystals for Windows* program.[42] Further details on the data collection, solution, and refinement are available in the Supporting Information.

(PNP)MnCl$_2$Li(THF)$_2$ (5). A solution of ^{n}BuLi (1.1 mmol) in hexanes (2.5 M) was added to a solution of **1** (430 mg, 1.00 mmol) in 2 mL of THF that was precooled to −35 °C in a freezer. The reaction mixture was allowed to reach room temperature and stirred for 1.5 h. Then, $MnCl_2$ (585 mg, 4.65 mmol) was added, and the solution was stirred for 12 h. The solution was filtered through Celite, and the solvent was evaporated to dryness, leaving the product as a bright yellow paramagnetic powder, which was washed with pentane and dried under vacuum (640 mg, yield 91%). Single crystals were grown from cooling a concentrated Et_2O solution to −35 °C; $\mu_{eff} = 5.8\ \mu_B$.

(PNP)MnCl (6). A solution of ^{n}BuLi (5.12 mmol) in hexanes (2.5 M) was added to a solution of **1** (2.00 g, 4.65 mmol) in 10 mL of THF that was precooled to −35 °C in a freezer. The reaction mixture was allowed to reach room temperature and stirred for 1.5 h. Then, $MnCl_2$ (0.585 g, 4.65 mmol) was added, and the solution was stirred for 12 h. The solution was filtered through Celite, and the solvent was evaporated to dryness, leaving a bright crystalline yellow paramagnetic powder of (PNP)MnCl$_2$Li(THF)$_2$ (**5**), which was washed with pentane and dried under vacuum. Repeated recrystallization of the bright yellow powder from THF/pentane with interim filtrations of the solutions through Celite resulted in the elimination of LiCl from **5** to give PNPMnCl (**6**) as a fine light yellow powder (2.10 g, 87%). Elem. An. Found (Calculated) for $C_{26}H_{40}NO_3P_2ClMn$: C, 60.32 (60.21); H, 7.74 (7.78); N 2.79 (2.70); Cl, 6.39 (6.35) %; $\mu_{eff} = 4.9\ \mu_B$.

(PNP)MnMe$_2$Li(THF)$_2$ (7). A solution of MeLi (0.385 mmol) in ether (1.6 M) was added to a solution of **6** (100 mg, 0.193 mmol) in 2 mL of THF that was precooled to −35 °C in a freezer. The yellow solution turned orange and was stirred overnight. The solution was filtered through Celite, and the solvent was removed under vacuum leaving behind a dark yellow oil. The oil was triturated with pentane and isooctane until it became solid. The yellow paramagnetic solid was recrystallized three times from THF/pentane (40 mg, 31%). Single crystals were grown from diffusion of pentane into a concentrated THF solution at −35 °C; $\mu_{eff} = 5.6\ \mu_B$.

(PNP)Mn(py)$_3$ (8). A 25 mL Schlenk flask was charged with NaK (1:1 ratio of Na to K, 36 mg, 0.58 mmol each Na, K), and a solution of **6** (137 mg, 0.264 mmol) in 3 mL of THF was added to it. After 5 min, pyridine (63 μL, 0.845 mmol) was added via a microsyringe. The solution immediately turned green, and some NaK was visibly consumed. The solution was stirred at room temperature for 30 min and then filtered through Celite. The solvent was removed under vacuum leaving a green oil that was recrystallized from THF/pentane. A green paramagnetic solid was obtained (80 mg, yield 42%). Elem. An. Found (Calculated) for $C_{41}H_{55}N_4P_2Mn$: C, 68.30 (68.36); H, 7.69 (7.61); N 7.77 (7.41)%; $\mu_{eff} = 5.22\ \mu_B$.

(PNP)Mn(bipy) (9). A 25 mL Schlenk flask was charged with Li metal (5.0 mg, 0.72 mmol) and 2,2′-bipyridine (112 mg, 0.720 mmol) in THF (3 mL). When all the solid Li metal was visibly consumed (ca. 5 min), **6** (374 mg, 0.722 mmol) was added, and the solution was stirred at room temperature for 4 h. The solution was filtered through Celite, and the solvent was removed under vacuum. The remaining solid was washed with pentane and recrystallized twice from THF/pentane. A brown paramagnetic solid (363 mg, yield 80%) was obtained. Single crystals were grown from diffusion of pentane into a concentrated THF solution at −35 °C. Elem. An. Found (Calculated) for $C_{36}H_{48}N_3P_2Mn$: C, 67.32 (67.58); H, 7.42 (7.57); N 6.52 (6.57)%; $\mu_{eff} = 4.5\ \mu_B$.

(PNP)Mn(bipy)(CO) (10). A 10 mL flask equipped with a PTFE vacuum valve was charged with **9** (100 mg, 0.156 mmol) and 3 mL of THF. The resultant solution was degassed, and 1 atm of CO was introduced in the flask. The solution was stirred at room temperature for 2 h; during this time the solution turned purple. The solution was filtered through Celite, and the solvent was removed under vacuum. The remaining purple solid was recrystallized from THF/pentane (96 mg, 92%). Single crystals were grown from diffusion of pentane into a concentrated THF solution at −35 °C. Elem. An. Found (Calculated) for $C_{36}H_{48}N_3OP_2Mn$: C, 66.56 (66.54); H, 7.43 (7.25); N 6.22 (6.29) %. IR (C_6D_6) ν(Mn-CO) 1815 (Mn-bipy) 1456, 1308, 1161 cm^{-1}. ^{1}H NMR (toluene-d_8), 223.2 K): δ 10.24 (s, 1H, bipy), 9.27(s, 1H bipy), 8.59 (brd, 2H, bipy), 7.78 (s, 2H, bipy), 7.36−6.64 (4H, partially covered by solvent, Ar−H), 6.53 (s, 2H, Ar−H), 6.10 (brd, 2H, bipy), 1.99 (s, 6H, Ar−CH_3), 1.81 (m, 4H, PC*H*Me$_2$), 1.34 (m, 6H, PCH*Me$_2$*), 1.12 (m, 6H, PCH*Me$_2$*), 0.95 (m, 6H, PCH*Me$_2$*) 0.58 (m, 6H, PCH*Me$_2$*). ^{13}C{^{1}H} NMR (C_6D_6): δ 161.8, (m, CN, 2C), 158.7 (bipy), 156.2, 154.4 (bipy), 152.9, 133.9 (br s, 2C), 131.3, 131.0, 130.6, 130.4, 123.6 (bipy), 123.4, 123.3, 122.8, (br s, 2C, bipy), 122.6 (bipy), 119.6 (bipy), 118, 7 (bipy), 117.9 (bipy), 117.2 (bipy), 25.3 (d, $J_{C-P} = 9.0$ Hz, PC*H*Me$_2$), 25.3 (br m), 23.5 (d, $J_{C-P} = 10.0$ Hz, PC*H*Me$_2$), 20.9 (br s, 2C), 20.5, 20.4, 19.8, 19.3, 19.3, 19.2, 17.8, 17.7. ^{31}P{^{1}H} NMR (C_6D_6): δ 68.0.

Acknowledgment. Support of this research by the NSF (CHE-0809522, CHE-0944634), the Welch Foundation (Grant A-1717), the Alfred P. Sloan Foundation (Research Fellowship to O.V.O.), the Dreyfus Foundation (Camille Dreyfus Teacher-Scholar Award to O.V.O.) is gratefully acknowledged. The National Science Foundation is also acknowledged for the partial support of this work through Grant CHE-0521047 for the purchase of a new X-ray diffractometer at Brandeis University. We are also indebted to Prof. Michael Hall (Texas A&M) for helpful discussions and to the Supercomputing Facility and the Laboratory for Molecular Simulation at Texas A&M University for computer time and software.

Supporting Information Available: Crystallographic information for **5**, **7**, **9**, and **10** in the form of CIF files, experimental details, ground spin state optimized structures of **9** and **10**, and geometric/energetic data from TPSS calculation. This material is available free of charge via the Internet at http://pubs.acs.org.

(37) Weigend, F.; Ahlrichs, R. *Phys. Chem. Chem. Phys.* **2005**, *7*, 3297.
(38) Weigend, F.; Häser, M.; Patzelt, H.; Ahlrichs, R. *Chem. Phys. Lett.* **1998**, *294*, 143.
(39) Schäfer, A.; Horn, H.; Ahlrichs, R. *J. Chem. Phys.* **1992**, *97*, 2571.
(40) *Apex2*, Version 2 User Manual, M86-E01078; Bruker Analytical X-ray Systems: Madison, WI, 2006.
(41) Altomare, A.; Cascarano, G.; Giacovazzo, G.; Guagliardi, A.; Burla, M. C.; Polidori, G.; Camalli, M. *J. Appl. Crystallogr.* **1994**, *27*, 435.
(42) Betteridge, P. W.; Carruthers, J. R.; Cooper, R. I.; Prout, K.; Watkin, D. J. *J. Appl. Crystallogr.* **2003**, *36*, 1487.